Journal of Materials Research and Technology 38 (2025) 637–642

Contents lists available at ScienceDirect

Journal of Materials Research and Technology

journal homepage: www.elsevier.com/locate/jmrt

Theoretical explanation and regulation method for the edge effect in the sintered joints of metal nanoparticles

Guannan Yang [a], Zebo Li [a], Zhihao Zhang [a], Junyi Lu [a], Yu Zhang [a], Guanghan Huang [a,*], Tianshuo Zhao [b,**], Chengqiang Cui [a]

[a] State Key Laboratory of Precision Electronic Manufacturing Technology and Equipment, Guangdong University of Technology, Guangzhou, 510006, China
[b] Department of Electrical & Electronic Engineering, The University of Hong Kong, 999077, Hong Kong, China

ARTICLE INFO

Handling editor: M Meyers

Keywords:
Edge effect
Nanocrystalline metal
Sintering
Bonding
Joining

ABSTRACT

A theoretical model is proposed to explain the edge effect observed in sintered metal nanoparticle joints, which are characterized by a relatively loose and porous structure near the joint edges. By modeling the metal particle slurry as a granular system that follows the Mohr-Coulomb criterion, an exponential stress distribution is predicted, with high pressure at the center and low pressure at the edges, which reasonably explains the origin of the edge effect. With this understanding, a geometrically constrained sintering process is further proposed to mitigate the edge effect by using a pre-cured resin sealing layer around the chip edges to suppress the lateral flow of the metal nanoparticle slurry. Experimental results show that the constrained sintering process leads to the formation of a dense and uniform sintering structure in the sintered joint that has a 90 % enhancement in overall shear strength.

The rapid evolution of the semiconductor industry towards smaller, denser, multifunctional devices has imposed stringent performance requirements on advanced packaging technologies, such as flip-chip bonding and 3D integrated packaging [1–3]. Because of their inherent physical properties, traditional tin-based solder interconnect materials are increasingly unable to meet the demanding specifications for high thermal conductivity, electrical conductivity, high mechanical strength, and high-temperature stability in packaging interconnects [4–6]. In this context, metal nanoparticle sintering technologies, particularly those utilizing copper and silver nanoparticles, have garnered significant attention due to their unique characteristics that offer both low-temperature sintering and high-temperature operation [7–9]. Enabled by their surface activity, metal nanoparticles can sinter at temperatures significantly below their melting points, yielding sintered structures that have mechanical properties and electrical and thermal conductivity values that are close to those of bulk metals [10]. These attributes position the sintering of metal nanoparticles as a promising method for forming reliable packaging interconnections in advanced electronics packaging applications.

Unlike traditional tin-based solders that achieve metallurgical bonding through melting-solidification processes, the sintering and interconnection of metal nanoparticles rely on solid-state diffusion to form sintering necks [11]. This diffusion-driven kinetic process necessitates specific combinations of temperature (180–300 °C), auxiliary pressure (1–20 MPa), and duration (a few to tens of minutes) for completion [12–14]. Some study indicates that more solid phase will retain in the central area under compression, as the fluidity of the liquid phase is higher than that of the solid phase [15]. Extensive experimental observations have revealed that, despite generally exhibiting satisfactory overall performance, metal nanoparticle sintered joints consistently demonstrate porosity defects concentrated near joint edges, a phenomenon termed the "edge effect" [16,17]. Although widely recognized, the underlying physical mechanisms of the edge effect remain theoretically unexplored, and viable solutions to address the edge effect are lacking. As a result, the edge effect significantly impairs the performance and reliability of metal nanoparticles in their applications.

In this study, we propose a novel analytical approach based on the physical model of granular systems with internal friction, rather than conventional fluid models, to investigate the mechanism of the formation of edge effects in the sintering process of metal nanoparticles. Our analysis reveals that the shear deformation of the particle system must overcome internal friction forces generated by normal compressive

* Corresponding author.
** Corresponding author.
E-mail addresses: ghan.huang@gdut.edu.cn (G. Huang), tszhao@hku.hk (T. Zhao).

https://doi.org/10.1016/j.jmrt.2025.07.265
Received 20 June 2025; Received in revised form 16 July 2025; Accepted 28 July 2025
Available online 29 July 2025

stress, resulting in an exponentially distributed stress field characterized by high pressure in the central region and low pressure at edge regions. This is the fundamental cause of the edge effect. Building upon this theoretical framework, we further develop a geometrically constrained sintering process that effectively suppresses edge effects by restricting lateral shear extrusion deformation of the particle layer. This innovation enables the formation of uniform and dense sintered structures with significantly enhanced mechanical strength. These findings could resolve the long-standing question regarding the physical origin of edge effects in metal nanoparticle sintering and provide a feasible strategy for suppressing edge effects in nanoparticle-based interconnections in future advanced electronics packaging applications.

We first analyze the causes of the edge effect from a theoretical perspective. Fig. 1a illustrates a typical sintering process for die bonding. During sintering, silver paste is applied onto the substrate, followed by placing the chips on top of the paste. In this example, silver nanoparticles serve as an example, but other metal nanoparticles could be used in the solder paste. By applying heat and pressure, the silver nanoparticles within the paste sinter together, bonding the chips to the substrate. Due to the applied pressure, the paste tends to flow sideways and be squeezed out from the edge of the chip. The thickness of the final sintering layer is several to tens of microns [17–20].

If the deformation behavior of the metal paste before sintering is modeled as that of a liquid, the paste is entirely extruded under pressure, contradicting experimental observations. Considering that metal paste is a mixture of metal particles and solvents, when the solid content is high, the internal friction between particles leads to yield deformation behavior resembling granular systems like sand. Therefore, we employ the Mohr-Coulomb criterion [21] to describe the deformation behavior of the metal paste:

$$\tau = c + \alpha\sigma \tag{1}$$

where τ is the shear strength along a shear plane, σ is the normal stress, α is the internal friction coefficient, and c is the cohesion force. In the stress state diagram, Mohr-Coulomb's law is expressed as a straight line, while the stress state at a point in the material can be represented by a Mohr's circle, as shown in Fig. 1b.

In Fig. 1c, we analyze the internal stress within the paste. The substrate is coated with metal paste and covered by a chip, with a downward pressure applied to the chip. A coordinate system is established with the chip edge as the origin to analyze the stress state of a local paste element at position x (indicated by the red box). The normal stress in the paste element along the y-axis is represented as σ_y, and the horizontal stresses along the x-axis on the two sides of the element are represented as σ_x and $\sigma_x + d\sigma_x$. Considering the extrusion of the paste under the pressure, there is a shear stress τ at the upper and lower surfaces of the paste. Based on force equilibrium in the horizontal direction, the following relationship holds:

$$2\tau dx = h d\sigma_x \tag{2}$$

where h is the thickness of the paste. Considering that the paste is being extruded away from the center, with lateral shear motion occurring at its upper and lower surfaces, the stress state meets the yield criterion. This can be represented in the stress space by the Mohr's circle being tangent to the Mohr-Coulomb criterion line, as illustrated in Fig. 1c. The abscissa and ordinate of the tangent point corresponds to σ_y and τ, respectively, which follow the Mohr-Coulomb criterion (Eq. (1)).

The opposite side of the Mohr's circle, which reflects the stress state on the plane oriented 90° to the shear plane, the abscissa corresponds to the horizontal stress σ_x in the element. Based on the geometric relationship shown in Fig. 1c,

$$\sigma_x = \sigma_y + 2\alpha\tau \tag{3}$$

Combining Eqs. (1)–(3) gives

$$2(\alpha\sigma_y + c)\partial x = h(1 + 2\alpha^2)\partial\sigma_y \tag{4}$$

Integrating results in

$$\sigma_y = \frac{1}{\alpha}\left[A e^{\frac{2\alpha x}{h(1+2\alpha^2)}} - c\right] \tag{5}$$

where A is an undetermined constant. Considering that there is no restraint at the edge of the chip, the stress tends to zero. Solving for A, we find $A = c$. Substituting A back into Eq. (5), we have:

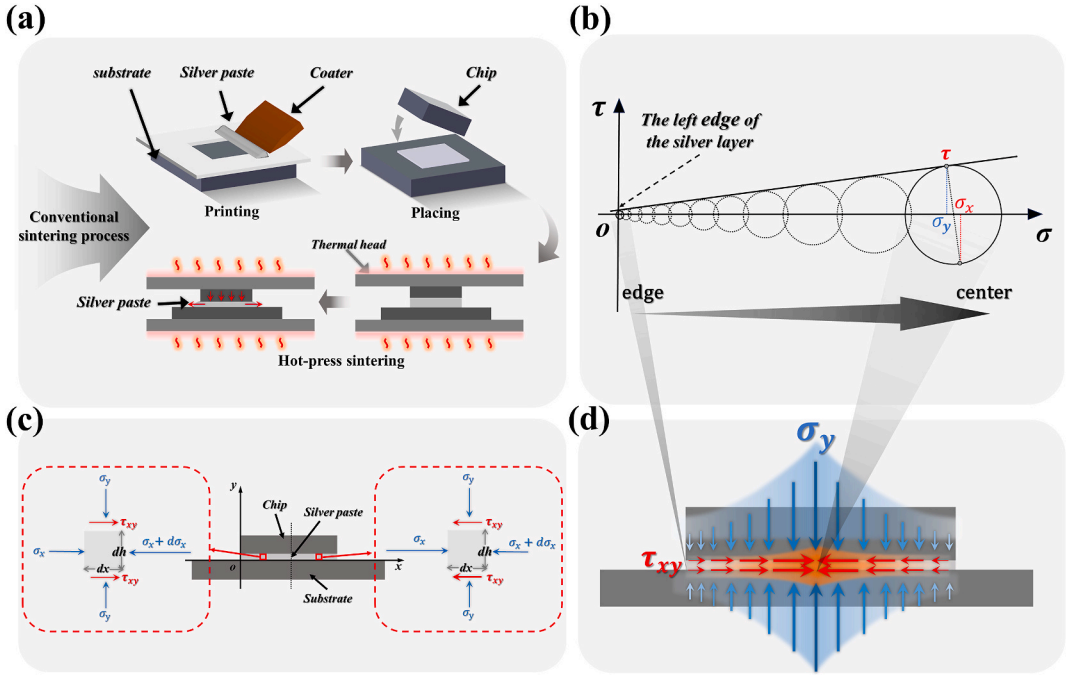

Fig. 1. (a) Traditional sintering procedures of metal nanoparticle pastes. (b) Illustration of the Mohr-Coulomb criterion and the stress state of the paste. (c) Stress analysis of a local paste element at position x. (d) Schematic diagram of the theoretical predicted stress distribution in the metal nanoparticle paste.

$$\sigma_y = \frac{c}{\alpha}\left[e^{\frac{2\alpha x}{(1+2\alpha^2)h}} - 1\right] \quad (6)$$

Eq. (6) represents the compressive stress distribution at different locations inside the paste.

Based on the above analysis, we drew a schematic diagram of the stress distribution of the metal nanoparticle paste during the sintering process, as shown in Fig. 1d. The value of σ_y increases exponentially from the edge to the interior of the sample and reaches a maximum near the center. Because τ maintains a linear relationship with σ_y (Eq. (1)), it follows a similar exponential growth pattern. The stress state of the paste region can be represented by a series of progressively enlarging Mohr circles tangent to the Mohr-Coulomb criterion line, as shown in Fig. 1b.

This stress distribution occurs because the Mohr-Coulomb criterion dictates that the deformation process of metal paste must overcome internal frictional resistance [21]. The lateral stress required for the central paste to reach the yield condition needs to overcome the integral of the frictional resistance from the center to the edge, resulting in higher pressure in the central region. In contrast, there is no lateral restriction near the edge of the chip, so only a very low stress is required to reach the yield condition. This ultimately forms a stress distribution pattern with minimal edge stress and maximum central stress. This theoretical derivation effectively explains the edge effect observed in sintered structures metal nanoparticle paste. The high pressure at the center facilitates sintering of metal particles, yielding a structure with low porosity [22,23]. Conversely, near-zero pressure at the edges leads to loose and porous structures after sintering [24].

It should be noticed that eq. (6) is valid to describe the pressure outside the center area. The stress state near the center is more complicated and is discussed in the supplementary material.

Based on the theoretical derivation above, we devised a sintering method with a geometric constraint designed to suppress the edge effect, as illustrated in Fig. 2. After coating silver paste on the substrate and mounting the chip, a ring of thermosetting epoxy resin is dispensed around the chip edges for sealing. The sample is heated to 130 °C without pressure to pre-cure the epoxy resin, followed by hot-press sintering at a higher temperature with pressure. The cured epoxy resin sealing layer acts as a geometric constraint, effectively inhibiting lateral extrusion of the silver paste and thereby suppressing the generation of the edge effect.

To test the devised sintering method, silver nanoparticles (purchased from Macklin Biochemical Technology Co., Ltd, Shanghai, China) with an average diameter of 60–120 nm were mixed with ethylene glycol to prepare a silver paste with a solid content of 80 wt % (corresponding to a volume fraction of 30 vol %) using a homogenizer (DACC 400.2 V, SpeedMixer) at a speed of 1500 rpm for 2 min. The paste was screen printed onto a 5 × 5 × 1 mm^3 copper plate, which represents the substrate. A separate 3 × 3 × 1 mm^3 copper plate that represented a chip was placed on top of the screen printed paste. Prior to use, the copper plates were cleaned with 5 vol% H_2SO_4 to remove the oxide layer on the surface. SC-A200 epoxy resin (purchased from Polybond Polymer Materials Co., Ltd, Guangzhou, China) was dispensed around the edge of the chip. Under vacuum, the sandwich structure was heated to 130 °C for 5 min to pre-cure the epoxy resin. Then a pressure of 2 MPa was applied to the chip and the temperature was raised to 260 °C for 30 min to sinter the silver paste. For comparison, a control group was processed using the traditional packaging method without resin was also performed under the same sintering conditions. After sintering, the shear strength of the samples was measured with a bonding tester (MFM-1200, TRY). The cross-sectional images of the samples were observed with a scanning electron microscope (SEM, SU8220, Hitachi).

Fig. 2b illustrates the method of determining the value of α. A sandwich-structured sample (copper plate–silver paste–copper plate) is placed on an adjustable inclined platform. The lower copper plate is

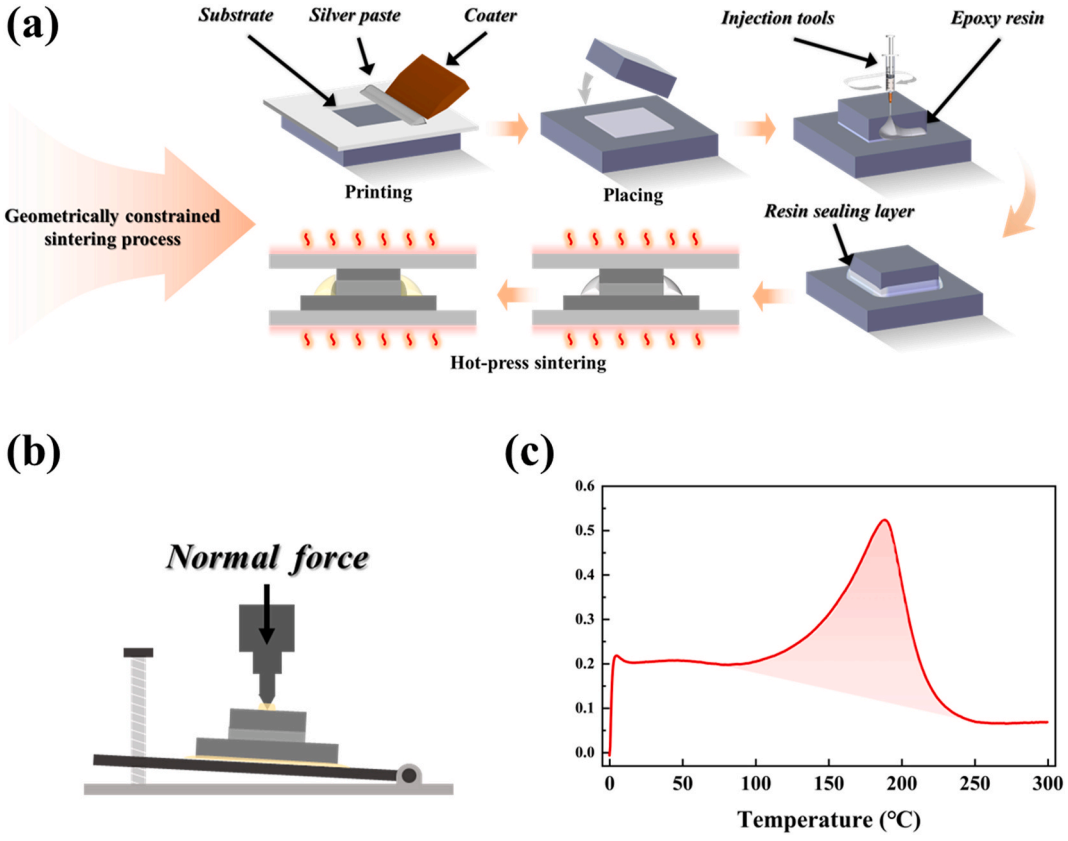

Fig. 2. (a) A sintering process with geometric constraint to suppress the edge effect. (b) Schematic of the method used to evaluate the internal friction coefficient α. (c) DSC curve of SC-A200 epoxy resin.

adhered to the surface of the platform. A relatively large constant normal load (10 N) is applied to the upper copper plate, ensuring no slippage occurs between the loading head and the upper copper plate. The platform's tilt angle is gradually increased from 0° until the upper copper plate begins to slide. The critical tilt angle θ is recorded, and the value of tanθ can be used to represent α. To ensure statistical reliability, the measurement is repeated five times and the average value is used.

The outgassing from the volatile components of the paste might create voids and inhibit the sintering process of the silver particles [25]. In this study, SC-A200 resin was selected as the encapsulation material due to its suitable curing temperature. The DSC curve of the SC-A200 resin was show below. The resin initiates pre-curing between 100 and 150 °C. During the sintering process, the sintered joint was heated at 130 °C for 5 min without pressure. At the moment, the resin is in the pre-cured state, so that a part of the organic solvent in the paste can be evaporated. Later, the joint was heated at 260 °C with a pressure of 2 MPa. The cured resin could also suppress the lateral extrusion of the silver paste at this stage. Thereby, a relatively uniform and compact sintering structure can be achieved.

Fig. 3a shows a cross-sectional view of the sintered silver joint fabricated by the conventional sintering process. The sintered layer exhibits very different densities at different positions. The structure near the edges of the sintered layer is porous and loose. The enlarged images indicate that there are still noticeable gaps between the particles. Sintering necks were not readily apparent, and the corresponding porosity of the cross-section was ~21.4 %. Closer to the center of the sample, more sintering necks are present between the particles, and the local density of the sintered layer increases significantly, reaching a maximum near the center with a porosity of ~4.8 %. This result confirms the existence of the edge effect. It shows that in the traditional sintering process the stress near the edge of the sample is low, and the applied pressure mainly affects the center of the sample, thus forming a density gradient in the sintered structure, with a compact middle and relatively loose grains at the edges.

The existence of the edge effect leads to a non-uniform sintered structure and a decrease in physical properties of the sintered joint. In contrast, because of the geometric constraint provided by the precured epoxy layer (Fig. 2), the lateral flow of the particle paste is limited, which fundamentally eliminates the cause of the edge effect. Fig. 3b shows a cross-sectional view of the sintered joint formed with the geometric constraint. The sintered layer shows a uniform and dense structure from the edge to the center. The enlarged images show that the metal particles at different positions in the sintered layer have formed thick sintering necks.

Eq. (6) provides a theoretical prediction of the pressure distribution inside the sintered layer. α is measured to be 0.038, and h is 27 μm. The applied pressure in the hot-press sintering process corresponds to an average of σ_y of 2 MPa, corresponding to a c of 5.2 kPa. Substituting the above parameters into Eq. (6), the pressure distribution and porosity at different positions inside the sintered layer are obtained, as shown in Fig. 4a. The porosity is consistent with the theoretically predicted pressure distribution, proving the validity of the theoretical prediction.

The porosity distribution of the sintered layer under geometric constraint is also shown in Fig. 4a. In contrast to the sample sintered

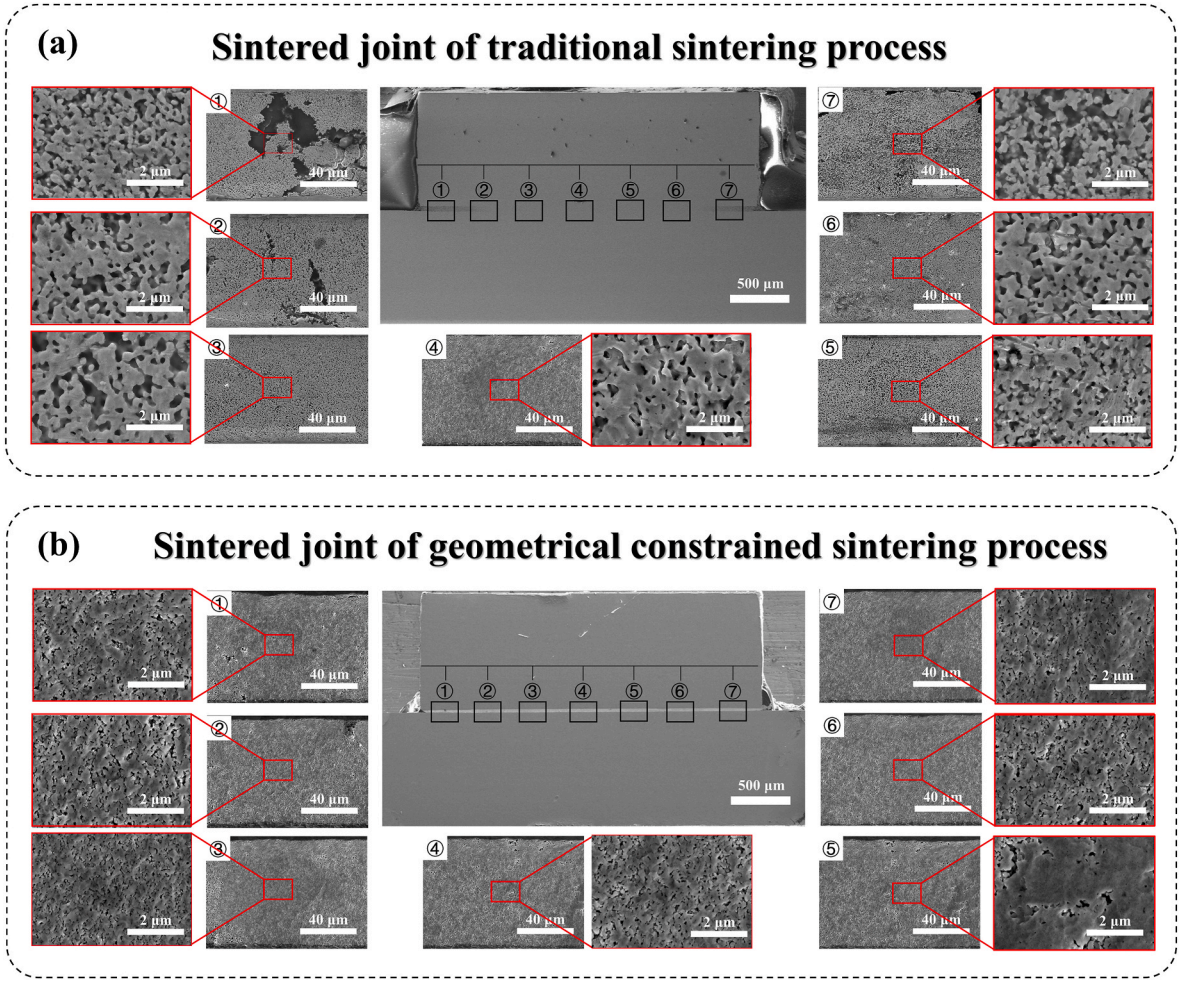

Fig. 3. (a) Cross-sectional SEM images of samples fabricated by the traditional sintering process. (b) Cross-sectional SEM images of samples fabricated under geometric constraint.

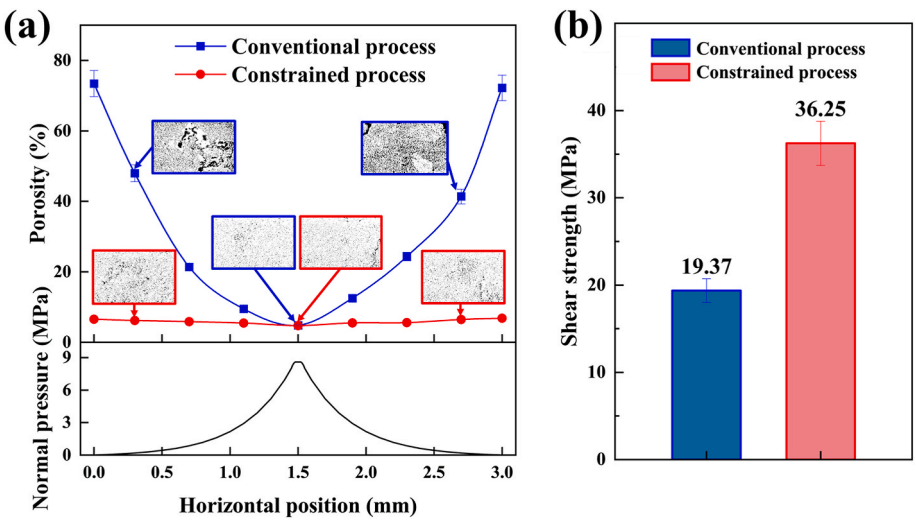

Fig. 4. (a) Porosity variation from the left to the right of the sintered layer in sintered joints fabricated by the traditional and optimized processes. (b) Shear strength of sintered joints fabricated by the traditional and optimized processes.

without a geometric constraint, the sample shows a very uniform, low porosity of ~5 %, which is close to the porosity at the center of the sintered joint under the conventional process. The shear strength of the samples sintered with and without geometric constraint is presented in Fig. 4b. The conventional process results in a strength of 19.3 MPa. The addition of the geometric constraint increases the strength by ~90 % to 36.25 MPa. This result proves that the geometric constraint can effectively suppress the generation of edge effect and thereby achieve a compact and uniform sintering structure with improved properties.

Based on the proposed model (Eq. (6)), when the coefficient of internal friction (α) and ratio of chip size to paste thickness (x/h) are low, there will be a smaller difference between the pressures in the center and near the edge of the joint. The internal friction coefficient of the silver paste ($\alpha = 0.038$) is relatively low and is close to some solid-liquid mixed systems such as magnetic fluid ($\alpha < 0.05$ [26]) and nanoparticle slurries ($\alpha = 0.03$–0.05 [27]). This exceptionally low friction characteristic can be attributed the lubricating effect of organic carriers. In comparison, conventional dry granular materials, such as sands or glass beads, typically exhibit a high α value ranging from 0.4 to 1.0 [28,29]. Cohesive particulate systems such as wet clays demonstrate intermediate values between 0.1 and 0.5 [30]. The usage of a metal paste with low solid content will be helpful to control the edge effect, as a low solid content corresponds to a low internal friction coefficient. In addition, the size, shape, and agglomeration of metal particles may also affect the internal friction coefficient. The effect of these factors on edge effect can be studied in the future. For the geometrically constrained process, metal or ceramic frames might achieve the same results. But in practical applications, it is difficult for these rigid frames to fit the chip size perfectly and to achieve tight adhesion with the joint to ensure the strength of the seal. In comparison, using epoxy resin for sealing is more convenient can could more flexibly fit the edge shape of the chips.

In summary, a theoretical model is proposed to explain the edge effect in sintered metal nanoparticle joints. With the conventional sintering process, the sintered structure near the joint edges is a relatively loose and porous. By treating the metal particle slurry as a granular system following the Mohr-Coulomb criterion rather than a liquid system, the model predicts an exponential stress distribution characterized by higher pressure at the center and lower pressure at the edges of the joint. This non-uniform stress distribution results from the internal friction force of the slurry during lateral shear flow. Based on this model, a sintering process with geometric constraints is proposed to address the nonuniformity in the sintered structure. Implementing a pre-cured resin sealing layer arround the chip edges effectively hinders lateral flow of the metal nanoparticle slurry and suppresses the edge effect. Experimental results demonstrate that the geometric constraint enables the formation of dense and uniform sintering structures at both the edges and the center, resulting in a 90 % increase in the overall shear strength applied to the joint. These findings provide theoretical and experimental foundations to understand and prevent edge effects in the formation of electrical interconnects with metal nanoparticles.

CRediT authorship contribution statement

Guannan Yang: Conceptualization, Methodology, Validation, Formal analysis, Writing – original draft, Writing – review & editing. **Zebo Li:** Data curation, Formal analysis, Investigation, Writing – original draft. **Zhihao Zhang:** Investigation. **Junyi Lu:** Investigation. **Yu Zhang:** Project administration. **Guanghan Huang:** Supervision, Funding acquisition. **Tianshuo Zhao:** Conceptualization, Methodology. **Chengqiang Cui:** Supervision, Funding acquisition.

Data availability

Data will be made available on request.

Declaration of competing interest

The authors declare that they have no known competing financial interests or personal relationships that could have appeared to influence the work reported in this paper.

Acknowledgments

This work was supported by the Guangdong S&T Programme (Grant No. 2023B0101020003, 2024B0101120004); the National Natural Science Foundation of China (Grant No. 62204063); the Science and Technology Program of Guangzhou (Grant No. 2025A04J5209); and the Guangdong Basic and Applied Basic Research Foundation (Grant No. 2024A1515011361, 2023A1515110642).

Appendix A. Supplementary data

Supplementary data to this article can be found online at https://doi.org/10.1016/j.jmrt.2025.07.265.

References

[1] Dai J, Wang Y, Grant T, Wang W, Mat M, Morshed M. High temperature reliability of pressureless sintered Cu joints for power SiC die attachment. Microelectron Reliab 2023;150:115219.

[2] Das Sharma D, Mahajan RV. Advanced packaging of chiplets for future computing needs. Nature Electronics 2024;7:425–7.

[3] Matsuda T, Seo R, Hirose A. Highly strong interface in Ag/Si sintered joints obtained through Ag2O–Ag composite paste. Mater Sci Eng, A 2023;865:144647.

[4] Zhang H, Lee N-C. Perspectives of high-temperature Pb-free bonding materials. International symposium on microelectronics, 2018; 2018. 000088-000098.

[5] Chen W, Liu X, Yang Z, Hu D, Liu X, Zhu X, Fan X, Zhang G, Fan J. Insights into sulfur and hydrogen sulfide induced corrosion of sintered nanocopper paste: a combined experimental and ab initio study. Mater Des 2024;240:112876.

[6] Kim S, Mhin S, Kim D. Driving force for enhancing the cold silver sinter joining using time domain-dependent Ag–Au epitaxy and interfacial stress. Mater Sci Eng, A 2024;909:146843.

[7] Yin L, Yang F, Bao X, Xue W, Du Z, Wang X, Cheng J, Ji H, Sui J, Liu X, Wang Y, Cao F, Mao J, Li M, Ren Z, Zhang Q. Low-temperature sintering of Ag nanoparticles for high-performance thermoelectric module design. Nat Energy 2023;8:665–74.

[8] Elmer JW, Specht ED. Direct observations of silver nanoink sintering and eutectic remelt reaction with copper. Scripta Mater 2010;63:1224–7.

[9] Li H, Qi Z, Yang G, Ding L, Li K, Wu F, Huang H. Atomistic study of shearing mechanism of nano-Ag joints and processing parameter optimization. Appl Surf Sci 2025;682:161757.

[10] Yoon S-S, Khang D-Y. Room-temperature chemical welding and sintering of metallic nanostructures by capillary condensation. Nano Lett 2016;16:3550–6.

[11] Yan J. A review of sintering-bonding Technology using Ag nanoparticles for electronic packaging. Nanomaterials 2021;11:4.

[12] Hu D, Cui Z, Fan J, Fan X, Zhang G. Thermal kinetic and mechanical behaviors of pressure-assisted Cu nanoparticles sintering: a molecular dynamics study. Results Phys 2020;19:1–10.

[13] Chen C, Zhao S, Sekiguchi T, Suganuma K. Large-scale bare Cu bonding by 10 μm-sized Cu–Ag composite paste in low temperature low pressure air conditions. J Sci Adv Mater Devices 2023;8:100606.

[14] Wang W, Wang M, Han L, Chen Y, Liu L, Yang F, Li M, Yu Z, Zhao Y. Low-resistance joints for YBCO-coated conductors with Ag nanoparticle paste. Supercond Sci Technol 2023;36:085016.

[15] Paknejad SA, Dumas G, West G, Lewis G, Mannan SH. Microstructure evolution during 300 °C storage of sintered Ag nanoparticles on Ag and Au substrates. J Alloys Compd 2014;617:994–1001.

[16] Gong H, Yao Y, Yang YT. Size effect on the fracture of sintered porous nano-silver joints: experiments and Weibull analysis. J Alloys Compd 2021;863:158611.

[17] Qian C, Sun Z, Fan J, Ren Y, Sun B, Feng Q, Yang D, Wang Z. Characterization and reconstruction for stochastically distributed void morphology in nano-silver sintered joints. Mater Des 2020;196:109079.

[18] Liu Y, Zhang H, Wang LG, Fan XJ, Zhang GQ, Sun FL. Effect of sintering pressure on the porosity and the shear strength of the pressure-assisted silver sintering bonding. IEEE Trans Device Mater Reliab 2018;18:240–6.

[19] Wu LM, Qian J, Yu JB, Guo HJ, Chen XP. Optimal Cu paste thickness for large-area Cu-Cu joint. Mater Lett 2021;291:129533.

[20] Chen C, Suganuma K. Large-scale ceramic–metal joining by nano-grained Ag particles paste sintering in low-temperature pressure-less conditions. Scripta Mater 2021;195:113747.

[21] Schuh CA, Lund AC. Atomistic basis for the plastic yield criterion of metallic glass. Nat Mater 2003;2:449–52.

[22] Tsai C-H, Huang W-C, Chew LM, Schmitt W, Li J, Nishikawa H, Kao CR. Low-pressure micro-silver sintering with the addition of indium for high-temperature power chips attachment. J Mater Res Technol 2021;15:4541–53.

[23] Xu H, Zou J, Wang W, Wang H, Ji W, Fu Z. Densification mechanism and microstructure characteristics of nano- and micro- crystalline alumina by high-pressure and low temperature sintering. J Eur Ceram Soc 2021;41:635–45.

[24] Zhou C, Zhong H, Lu H, Pang X, Zhang C, Wang H, Cong Q, Song Y, Shi N, Zhao J, Meng X, Chen J. Sintering pressure effect on the performances of near-zero thermal expansion xLFCS/Cu metal matrix composites. Ceram Int 2023;49:27958–64.

[25] Zhang Y, Liu Q, Liu Y, Tong J, Huang Z, Wu S, Liang P, Yang G, Cui C. Green synthesis of novel in situ micro/submicron-Cu paste for semiconductor interconnection. Nanotechnology 2022;33:285705.

[26] Song W-L, Choi S-B, Choi J-Y, Lee C-H. Wear and friction characteristics of magnetorheological fluid under magnetic field activation. Tribol Trans 2011;54:616–24.

[27] Kader A, Selvaraj V, Ramasamy P, Senthilkumar K. Experimental investigation on the thermo-physical properties and tribological performance of acidic functionalized graphene dispersed VG-68 hydraulic oil-based nanolubricant. Diam Relat Mater 2023;133:109740.

[28] Cortés R, Martínez MA, Navarro C, Sánchez-Gálvez V. Measurements of internal friction coefficient of SiC and Al2O3 powders. J Mater Sci 2004;28:6737–40.

[29] Skuodis Š, Norkus A, DirgĖLienĖ N, Rimkus L. Determining characteristic sand shear parameters of strength via a direct shear test. J Civ Eng Manag 2016;22:271–8.

[30] Odacıoğlu OG, Doğan O. An experimental study to determine sliding shear strength and internal frictional coefficient of clay brick wall in A masonry building. Uluslararası Muhendislik Arastirma ve Gelistirme Dergisi 2019:670–6.